Structure of Micelles of Poly(*n*-butyl acrylate)-*block*-poly(acrylic acid) Diblock Copolymers in Aqueous Solution

Olivier Colombani,† Markus Ruppel,† Markus Burkhardt,† Markus Drechsler,† Manuela Schumacher,† Michael Gradzielski,‡ Ralf Schweins,§ and Axel H. E. Müller*,†

Makromolekulare Chemie II and Bayreuther Zentrum für Kolloide und Grenzflächenforschung, Universität Bayreuth, D-95440 Bayreuth, Germany; Stranski-Laboratorium für Physikalische und Theoretische Chemie, Institut für Chemie, Technische Universität Berlin, Strasse des 17. Juni 124, D-10623 Berlin, Germany; and Institut Laue-Langevin, LSS group, 6 rue Jules Horowitz, F-38042 Grenoble, France

Received April 30, 2006; Revised Manuscript Received March 29, 2007

ABSTRACT: We report the structure and dynamics of micelles of the amphiphilic diblock copolymers poly(*n*-butyl acrylate)-*block*-poly(acrylic acid) (P*n*BA−PAA). These self-assembled nanostructures consist of a liquid hydrophobic core and a pH- and ionic strength-sensitive hydrophilic corona. In the first part of this series,[1] we reported the synthesis and micellization of these block copolymers in aqueous media without the need of any cosolvent. Here we present a detailed study on the structural and dynamic properties of these micelles in aqueous solutions under various conditions using static and dynamic light scattering (SLS, DLS), small-angle neutron scattering (SANS), and cryogenic transmission electron microscopy (cryo-TEM). The block copolymers spontaneously dissolve in water, forming rather monodisperse micelles. Although the corona thickness depends on external stimuli, such as pH and salinity, the micelles do not significantly change their shape or aggregation number upon modifications of these parameters, in spite of the liquidlike nature of the hydrophobic block at room temperature. Moreover, the structure of the formed micelles depends on the preparation conditions: aggregates of micelles are initially formed when the polymers are dissolved in saline aqueous solutions even at pH 6.5, which disintegrate within weeks, resulting in isolated micelles with significantly larger size compared to micelles at the same ionic strength but initially prepared in the absence of added salt. The results are explained in terms of a kinetic control of the micellization process, which is dynamic in terms of unimer exchange but slow on the experimental time scale in adapting to external stimuli.

Introduction

As outlined in our previous paper,[1] there is strong interest in amphiphilic block copolymers consisting of a soft hydrophobic block and a weak ionic block. "Frozen" micelles, such as those obtained from polystyrene-*block*-poly(acrylic acid) (PS−PAA)[2] in aqueous media, are only formed by dissolving the polymer with the help of a nonselective cosolvent or by prolonged heating of the solution above the glass transition temperature, T_g, of the hydrophobic block. In contrast, "dynamic" micelles are expected to be formed by block copolymers with a liquidlike hydrophobic block, which may spontaneously self-assemble into micellar structures in aqueous solutions without the need of any cosolvent. Furthermore, the aggregation characteristics of such micelles may be tuned by external stimuli such as pH and ionic strength. In dynamic micelles, unimer exchange is a prerequisite to enable the micelles to be in equilibrium with their free unimers in solution.

Förster et al. first reported on the study of micelles with a soft polyethylethylene (PEE) core and poly(styrenesulfonic acid) (PSS) corona.[3−5] They found that the degree of aggregation of the self-assembled structures strongly depends on the concentration of added salt. However, the strong polyacid does not allow for a pH dependence of the micellar size. Polyisobutylene-*block*-poly(methacrylic acid) (PIB−PMAA) with a short to medium hydrophobic PIB segment (degree of polymerization, DP_{PIB} = 25−75), and a long weak ionic hydrophilic block PMAA ($DP_{PMAA} > 100$) is spontaneously soluble in water and yields dynamic micelles.[6,7] On the contrary, the same diblock copolymers with a significantly longer hydrophobic block only self-assemble into micelles with the help of a cosolvent.[8] Since in both cases the nonionic block is very hydrophobic, it is of interest to study whether the polarity of that block has an effect on the self-organization of amphiphilic block copolymers. Poly(*n*-butyl acrylate), having a higher polarity and a low T_g of −55 °C, appeared to be a good candidate for this.

In our previous paper,[1] we reported the synthesis of well-defined poly(*n*-buyl acrylate)-*block*-poly(acrylic acid) (P*n*BA−PAA) diblock copolymers with polydispersity index PDI < 1.07 by atom transfer radical polymerization (ATRP) of *n*-butyl acrylate and *tert*-butyl acrylate (*t*BA), followed by selective and quantitative acidolysis of the P*t*BA block into poly(acrylic acid). The P*n*BA blocks have almost constant length (DP_{PnBA} = 90−100), whereas the PAA block lengths vary (DP_{PAA} = 33, 100, 150, 300). The polymers with $DP_{PAA} \geq 100$ are directly soluble in water of pH > 4.7 (corresponding to a degree of ionization, $\alpha > 0.2$). Fluorescence correlation spectroscopy (FCS) proved the formation of supramolecular structures in aqueous solution which were assigned to micelles, since their hydrodynamic radii, R_h, range from 25 to 50 nm. FCS and steady-state pyrene fluorescence spectroscopy indicated a very low "apparent" critical micellar concentration, cmc* $\sim 10^{-8}$ mol/L, for all polymers in the absence and presence of added salt at high pH ($\alpha = 1$). FCS also revealed a gradual decrease of the micellar hydrodynamic radii on dilution in the absence of salt. This was attributed to a dynamic, but kinetically controlled, behavior of these self-assembled nanostructures.

* Corresponding author: Ph +49-921-553399, Fax +49-921-553393, e-mail axel.mueller@uni-bayreuth.de.
† Universität Bayreuth.
‡ Technische Universität Berlin.
§ Institut Laue-Langevin.

10.1021/ma0609580 CCC: $37.00
Published on Web 05/16/2007

Here we report an extensive study on the aqueous solution properties of the micelles that are spontaneously formed by the P*n*BA−PAA block copolymers, in order to gain a deeper insight into the unexpected self-aggregation behavior of this system. Various scattering methods and cryogenic transmission electron microscopy were exploited to characterize the self-assembled micellar structures as a function of PAA block length, pH, ionic strength, and preparation conditions.

Experimental Section

Preparation of the Aqueous Polymer Solutions. The aqueous solutions were prepared using Millipore water (deionized water, resistance > 18 MΩ), sodium chloride (99.5%, Fluka), tris(2-amino-2-hydroxymehtyl-1,3-propanediol) (TRIS, Aldrich, 99.8%), HCl (0.01, 0.1, or 1 M), and NaOH (0.01, 0.1, or 1 M). NaOH and HCl solutions were prepared using Titrisol concentrated solutions, and NaOH solutions were back-titrated with HCl before use. The pH was measured using a glass electrode connected to a Schott pH-meter CG 840 calibrated with two buffer solutions at pH 4.0 and 10.0. A third buffer at pH 7.0 was used to check the accuracy of the pH-meter.

The aqueous copolymer solutions at a degree of ionization of the PAA block, $\alpha > 0.2$, and in the presence of added NaCl, were made following two different methods. Method 1 consisted of dissolving the polymer in pure water with an appropriate quantity of NaOH to control α and adding NaCl after at least one night to ensure complete dissolution of the polymer. For method 2, the polymer was directly dissolved in the presence of NaCl at the desired α value by adding an appropriate amount of NaOH.

For α values lower than 0.2, the polymer was first dissolved at $\alpha \sim 1$ in pure water. After one night, the desired α and salt concentration were adjusted by first adding HCl and then NaCl. This latter procedure was only used for solutions studied by SLS, which were dialyzed before analysis. The salt created when correcting α from 1 to 0 was thus no important issue, since the final salt concentration was adjusted by dialysis.

Static Light Scattering (SLS). For each SLS measurement, a stock solution was first prepared using method 1 or 2 at the desired α value and NaCl concentration and at a polymer concentration of 2.0 g/L. The stock solution was dialyzed in a cellulose dialysis membrane (Spectrapor7, molecular weight cutoff = 1000 g/mol) for 5−7 days against about 30 times as much water having the same pH and NaCl concentration as the polymer stock solution.[9,10] Each of the six solutions was filtered three times through nylon filters (13-HV, Millipore, 0.45 μm pore size) into cylindrical quartz scattering cells (1 cm diameter) at least one night before the measurement. Measurements were performed with a Sofica goniometer (He−Ne laser, $\lambda = 632.8$ nm) at 23 °C after calibration with filtered toluene. The background was measured with filtered water, since no significant difference was observed when the dialyzate was used as background. The refractive index increment (d*n*/d*c*) of the polymer in the studied solutions was determined at 23 °C on a Chromatix laser differential refractometer KMX-16 using the dialyzate as reference. M_w, R_g, and A_2 values were finally determined using a Zimm plot of the data whenever valid.

Dynamic Light Scattering (DLS). If solutions were studied both by DLS and SLS, the solution at a polymer concentration of 0.5 g/L used for SLS was used without modification for DLS. Otherwise, solutions were freshly prepared using method 1 or 2 and measured without dialysis. A small difference of R_h was observed for P*n*BA$_{90}$−PAA$_{300}$ solutions prepared either with or without dialysis. This may be explained by a change of the NaCl concentration in the bulk solution during dialysis. All solutions were filtered three times through nylon filters (13-HV, Millipore, 0.45 μm pore size) into cylindrical quartz scattering cells (1 cm diameter) one night prior to measurement. Some solutions prepared with method 1 at $\alpha \sim 1$ were also filtered with 0.20 μm filters, and it was checked that this made no significant difference. The DLS measurements were carried out at scattering angles ranging from 30° to 150° with an ALV DLS/SLS-SP 5022F equipment consisting of an ALV-SP 125 laser goniometer, an ALV 5000/E correlator processing in cross-correlation mode, and a He−Ne laser ($\lambda = 632.8$ nm).

The regularized Laplace inversion (CONTIN procedure) was applied to analyze the obtained autocorrelation functions. The *z*-average hydrodynamic radius, R_h, at each angle was determined using the intensity-weighted distribution of particle sizes. The R_h values were extrapolated to $q^2 = 0$ when there was a (linear) dependence on q^2. Otherwise, R_h values at 30° and 150° are given to demonstrate the angular dependence.

Small-Angle Neutron Scattering (SANS). Polymer solutions were prepared at 1 g/L, using D_2O (99.98%, Aldrich) instead of H_2O in order to maximize the contrast in SANS and controlling the degree of ionization by addition of a D_2O solution of NaOH back-titrated with a 0.1 M aqueous HCl solution. Solutions of P*n*BA$_{100}$−PAA$_{150}$ and P*n*BA$_{90}$−PAA$_{300}$ without added salt are very viscous, whereas they become fluid upon addition of NaCl. All salt-containing solutions were prepared using method 1. Measurements were performed at instrument D11 at the Institut Laue−Langevin (ILL) in Grenoble, France. Scattering intensities were recorded with a two-dimensional position-sensitive ^{3}He detector. Four different instrument settings were used: sample−detector distances of 1.1, 4, and 16 m with a neutron wavelength of 6 Å and a sample−detector distance of 34 m with a neutron wavelength of 10 Å. This corresponds to a momentum transfer range of $0.0012 < q < 0.33$ Å^{-1}. All samples were measured in 2 mm Hellma quartz cells at room temperature. H_2O serving as calibration standard was filled into a 1 mm Hellma cell. After determination of the central detector coordinates for each sample−detector distance, the two-dimensional raw data were radially averaged. Averaged data were normalized by use of the known wavelength-dependent effective differential cross section of H_2O.[11] The transmission of the samples was determined by measuring the direct, attenuated, incident beam (I_i) at zero momentum transfer, divided by the respective measurement of the incident beam passing through any object (I_x), $T_x = I_x(q=0)/I_i(q=0)$. The differential scattering cross section per unit volume of the solutions and the solvents was separately calculated according to the following equation:[11]

$$\left(\frac{d\Sigma}{d\Omega}\right)_S = \frac{(I_S - I_{Cd}) - \dfrac{T_{S+EC}(1 - n_S\tau)}{T_{EC}(1 - n_{EC}\tau)}(I_{EC} - I_{Cd})}{(I_{H_2O} - I_{Cd}) - \dfrac{T_{H_2O+EC} + (1 - n_{H_2O}\tau)}{T_{EC}(1 - n_{EC}\tau)}(I_{EC} - I_{Cd})} \times \frac{T_{H_2O+EC} + (1 - n_{H_2O}\tau)0.1\left(\dfrac{d\Sigma}{d\Omega}\right)_{H_2O}}{T_{EC}(1 - n_{EC}\tau)\cdot 0.2} \quad (1)$$

The indices denote sample (S), corresponding to solvents or solutions, standard (H_2O), empty cells (EC), and cadmium (Cd). The cadmium measurement provides the electronic background. The term $(1 - n\tau)$ is a first-order correction for dead time losses with n being the integral count rate of each measurement and τ being the dead time. It should be noted that this differential cross section, i.e., the absolute intensities we used, still contains the incoherent background scattering of the sample.

The scattering curves were analyzed mainly by fitting a form factor to the high q range, which is not significantly affected by the structure factor that is due to the interactions between the charged aggregates. For all the samples of this study, this condition is given for $q > 0.02$ Å^{-1}. As the simplest model we employed that of polydisperse spheres with a homogeneous scattering length density. In our case, the spheres correspond to the dense hydrophobic core of the micelles, which is supposed to be made up principally from P*n*BA but in some cases ($\alpha \leq 0.75$) has a dense shell of partially collapsed PAA at the core−corona interface. The part of PAA in this shell is determined by the increase of the scattering intensity of the core (which also leads to a slight modification of the scattering length density difference, $\Delta\rho$, which

was taken into account in a self-consistent manner). For such a model the scattering intensity is given by

$$I(q) = {}^1N \int_0^\infty f(R_c,\langle R_c\rangle)\, P(q,R_c)\, \mathrm{d}R_c \tag{2}$$

where ${}^1N$ is the number density of micellar aggregates and $P(q,R_c)$ is the form factor of a monodisperse homogeneous sphere of radius R_c (radius of the hydrophobic core of the aggregate), which can by written as

$$P(q,R_c) = |F(q,R_c)|^2 = V_p{}^2\Delta\rho^2\left\{\frac{3(\sin(qR_c) - qR_c\cos(qR_c))}{(qR_c)^3}\right\}^2 \tag{3}$$

$f(R_c)$ is the distribution of the radii for which we employed a Schulz distribution:[12]

$$f(R_c,\langle R_c\rangle) = \left(\frac{Z+1}{\langle R_c\rangle}\right)^{Z+1}\frac{R_c{}^z}{\Gamma(Z+1)}\exp\left(-\frac{(Z+1)R_c}{\langle R_c\rangle}\right) \tag{4}$$

which is characterized by the polydispersity index p:

$$p^2 = \frac{\langle R_c{}^2\rangle}{\langle R_c\rangle^2} = \frac{1}{Z+1} \tag{5}$$

$\Delta\rho$ is the difference between the scattering length density of the core, ρ_c, and the solvent, ρ_s, where we employed $\rho_c = 5.8 \times 10^9$ cm^{-2} (P*n*BA) (and 15.9×10^9 cm^{-2} for PAA when we considered a part of the PAA to be collapsed onto the micellar core) and $\rho_s = 63.5 \times 10^9$ cm^{-2} (D_2O).

This relatively simple model already yields a very good fit for the scattering intensity, and it was verified that including the scattering of the corona by means of a scattering length density that decreases by $1/R$ does not lead to any systematic changes of the parameters deduced. From the core radius, the aggregation number can be calculated via eq 6

$$m_{core} = \frac{4\pi}{3}\rho R_{core}{}^3 = N_{agg}\frac{M_{PnBA}}{N_A} \tag{6}$$

where M_{PnBA} is the molecular weight of the hydrophobic P*n*BA block, N_A is the Avogadro's number, and ρ is the bulk density of the P*n*BA in the core (measured to be 1.04 g/cm^3 at 20 °C for P*n*BA$_{90}$).

The errors in parameters obtained by DLS, SLS, or SANS for strongly scattering systems such as polymeric micelles is generally agreed to be in the range 10−20%. This error will be considered when discussing values obtained in the same conditions by different methods. However, since all DLS experiments (respectively SLS or SANS) were done using the same apparatus under the same conditions, data obtained with this method might be compared to each other with a significantly smaller error. We will thus consider a difference of 10% (which corresponds to an error of 5%) to be significant when comparing data obtained from two methods (respectively DLS, SLS or SANS).

Cryogenic Transmission Electron Microscopy (Cryo-TEM). Some of the solutions at 0.5 g/L prepared for DLS or SLS were analyzed by cryo-TEM without filtration. A drop of the sample was put on an untreated bare copper TEM grid (600 mesh, Science Services, München, Germany), where most of the liquid was removed with blotting paper leaving a thin film stretched over the grid holes. The specimens were instantly shock vitrified by rapid immersion into liquid ethane cooled at ~90 K by liquid nitrogen in a temperature-controlled freezing unit (Zeiss Cryobox, Zeiss NTS GmbH, Oberkochen, Germany). The temperature was monitored and kept constant in the chamber during all the sample preparation steps. After freezing a specimen, the remaining ethane was removed using blotting paper. The specimen was inserted into a cryo-transfer holder (CT3500, Gatan, München, Germany) and transferred to a Zeiss EM922 EF-TEM (Zeiss NTS GmbH, Oberkochen, Germany). Examinations were carried out at ~90 K. The TEM was operated at an acceleration voltage of 200 kV. Zero-loss filtered images ($\Delta E = 0$ eV) were taken under reduced dose conditions (approximately 100−1000 e/nm^2). All images were registered digitally by a bottom-mounted CCD camera system (Ultrascan 1000, Gatan) combined and processed with a digital imaging processing system (Digital Micrograph 3.10 for GMS 1.5, Gatan). The core of ~100 micelles was measured manually for the determination of the number-average core radius, R_c. The error on the determination of the diameter of the core is mainly due to the qualitative estimation of the limit of the core region and was estimated to be 1 nm (which corresponds to an error of 0.5 nm on R_c).

Results and Discussion

Among the four diblock copolymers, the synthesis of which was previously reported,[1] the one consisting of the shortest PAA block (P*n*BA$_{90}$−PAA$_{33}$) is not directly soluble in water. Thus, only the three most hydrophilic block copolymers (P*n*BA$_{90}$−PAA$_{100}$, P*n*BA$_{100}$−PAA$_{150}$, and P*n*BA$_{90}$−PAA$_{300}$) will be considered in this article. Micellar solutions of these block copolymers were investigated in two different ways.

The influence of different parameters (PAA block length, ionic strength, and pH) is detailed in the first three sections of the present article. For these studies, the block copolymers were dissolved using the method 1 of preparation described in the Experimental Section; i.e., the polymer is first dissolved in the absence of added salt at the desired pH, and NaCl is added after one night of equilibration. This method indeed proved to enable a fast and reproducible dissolution of the block copolymers under the formation of monodisperse micelles. Moreover, the micellar solutions do not seem to change within several weeks, which makes it possible to compare the different experiments independently of the elapsed time between the preparation of the solution and their analysis.

In the fourth section of this paper, the influence of the preparation conditions of the micellar solutions on the characteristics of the micelles was studied, and method 1 was compared to a second method of solution preparation (method 2), where the polymer was dissolved directly in an aqueous salt solution.

1. Effect of the PAA Block Length. Static and dynamic light scattering (SLS and DLS) experiments were performed in the presence of 0.1 M NaCl at pH ~ 7, corresponding to a degree of ionization, $\alpha \sim 0.9$. Zimm plot analysis of the results yielded the weight-average molecular weight, M_w, the z-average radius of gyration, R_g, and the second virial coefficient, A_2 (Table 1). A representative Zimm plot for all polymer solutions prepared with method 1, at pH ≥ 5.5, and with 0.1 M NaCl, is shown later (Figure 14, left). The solution at a polymer concentration of 0.5 g/L was also analyzed by DLS to obtain the z-average hydrodynamic radius, R_h, of the micelles after CONTIN analysis (Figure 1 and Table 1; see also Figure 6). The degrees of aggregation, N_{agg}, derived from M_w are given in Table 2 and compared to values obtained by other methods.

The CONTIN plots reveal a rather narrow size distribution of the micelles. The hydrodynamic radii of all polymers do not depend on the magnitude of the scattering vector, which hints to spherical micelles. This hypothesis is supported by the ratios R_g/R_h (Table 1), which are in between the value of 0.775 for hard spheres and 1.78 for Gaussian coils in a good solvent. Moreover, these ratios are close to the value of 1.08 for star-shaped molecules[13] with a high arm number, i.e., starlike micelles with a high segment density of micellar arms (owing to a high aggregation number), and a small core with respect to the hydrophilic corona. The R_g/R_h values increase with

Table 1. SLS and DLS Results for the Micelles Formed by the Diblock Copolymers at pH ~ 7 (α ~ 0.9) and 0.1 M Added NaCl (Dissolution Using Method 1)

	d*n*/d*c* (mL/g)[a]	$10^{-6}M_w$[b] (g/mol)	10^6A_2[c] (mol mL/g^2)	R_g[b] (nm)	R_h[c] (nm)	p[d]	$R_{h,n}$[e] (nm)	R_g/R_h
P*n*BA$_{90}$−PAA$_{100}$	0.167	9.1	7.4	31	32	0.06	21	0.95
P*n*BA$_{100}$−PAA$_{150}$	0.169	9.8	13	45	43	0.09		1.05
P*n*BA$_{90}$−PAA$_{300}$	0.192	10.7	43	65	56	0.09	39	1.16

[a] By differential refractometry using the dialyzate as reference. [b] By SLS, from a Zimm plot. [c] *z*-average determined by DLS at $c = 0.5$ g/L. [d] Polydispersity $p = \mu_2/G^2$ determined by the cumulant method at scattering angle $\theta = 90°$. [e] Number average obtained by FCS at ~1 g/L.[1]

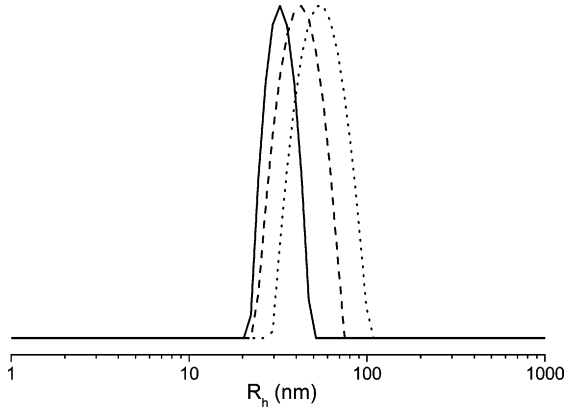

Figure 1. Intensity-weighted CONTIN plots at scattering angle Θ = 90° for P*n*BA$_{90}$−PAA$_{100}$ (—), P*n*BA$_{100}$−PAA$_{150}$ (- - -), and P*n*BA$_{90}$−PAA$_{300}$ (···) at pH ~ 7 and 0.1 M NaCl (preparation according to method 1).

increasing PAA block length, which can be attributed to the fact that, for the shortest PAA block, the spherical core has a larger contribution, whereas the corona chains become more flexible at higher chain lengths.

Cryogenic transmission electron microscopy (cryo-TEM) micrographs (Figure 2) confirm the spherical shape of the micelles with a rather low dispersity. Because of the low contrast of the corona, only the core is seen in most images. The image of the P*n*BA$_{90}$−PAA$_{300}$ micelles indicates regular structures, which are a result of the electrostatic repulsion of the stretched PAA corona (close to overlap) with a hydrodynamic radius of 56 nm compared to 30 nm for P*n*BA$_{90}$−PAA$_{100}$. It should be noted that the concentration given may change during the blotting process; moreover, the thickness of the vitrified film is not constant.

Small-angle neutron scattering (SANS) experiments were also performed at different degrees of ionization, α, and salt concentrations (Figures 3−5). First we will only focus on the experiments at α ~ 1 and 0.1 M NaCl, which complement the DLS and SLS data at similar conditions. Typically, the SANS profiles for a given polymer look very similar, especially for $q > 0.03$ Å^{-1} (only the samples with very low degree of ionization exhibit some differences, as will be discussed later). The scattering at large q is dominated by the hydrophobic core, which is basically identical in size and polydispersity for the different samples of a given polymer. The analysis of the SANS data by fitting a form factor of polydisperse spheres according to eqs 2−4 (a representative fit is shown on Figure 3b) yielded the number-average core radius ($R_{c,SANS}$). The SANS results are in good agreement with data obtained by SLS and cryo-TEM (Table 2).

Data obtained by SANS, SLS, and DLS revealed a more detailed picture of the fully ionized micelles in saline solution (Table 2): the weight-average aggregation number, N_{agg}, of the micelles was calculated with SLS by dividing their M_w by the molecular weight of a single chain. Then, $R_{c,SLS}$, was calculated from $N_{agg,SLS}$ according to eq 6. $N_{agg,SANS}$ was calculated using $R_{c,SANS}$ and the same equation. Finally, the thickness of the hydrophilic corona was calculated as $d_{corona} = R_h - R_{c,SANS}$ and compared to the contour length of a fully extended PAA chain, $L_{contour,PAA} = DP_{PAA} \times 0.25$ nm. Since all polymers possess an almost constant P*n*BA block, those parameters could be represented as a function of the PAA block length in order to determine the influence of the PAA block (Figure 6).

All aggregation numbers are quite high and slightly decrease with increasing length of the PAA block length. However, taking the scatter into account, the DP range cover is not large enough to determine a reliable scaling exponent. The size of the micelles increases with longer PAA blocks because the hydrophilic corona becomes thicker: $R_g \propto DP_{PAA}^{0.6}$, $R_h \propto DP_{PAA}^{0.5}$, $d_{corona} \propto DP_{PAA}^{0.7}$. The decrease of N_{agg} with DP_{PAA} is in qualitative agreement with an increasing head group area due to the longer PAA block and thereby conforms to the generally observed trends in surfactants as they are explained by the packing parameter concept for spheres. Taking into account that we only have three data points in a rather small range, our R_h exponent comes close to that reported by Förster et al.,[14] $R_h \propto N_B^{0.44}$, where N_B is the degree of polymerization of the solvophilic block.

Finally, from the diameter of the corona, it can be deduced that the PAA chains are extended to 60−90% of their contour length, $L_{contour}$. This strong stretching is to be explained by the brushlike density of the chains and the repulsion of the negatively charged PAA blocks.[15] The ionic strength of the added 0.1 M NaCl is not high enough to provide complete screening of charges.

2. Effect of the Salt Concentration. In the following section, the effect of the salt concentration at full ionization is outlined for P*n*BA$_{90}$−PAA$_{100}$ (pH ~ 9−10) and P*n*BA$_{90}$−PAA$_{300}$ (pH ~ 11).

Cryo-TEM imaging of P*n*BA$_{90}$−PAA$_{100}$ at different salt concentrations (Figures 2 (left) and 7) reveals the spherical shape of micelles irrespective of the salt concentration up to 0.1 M NaCl. Moreover, both cryo-TEM (Figures 2 and 7) and SANS (Figures 4 and 5) prove that the R_c of the different block copolymers, and thus N_{agg}, is not significantly influenced by the salt concentration from 0 to 1 M (Table 3). The addition of

Table 2. Other Characteristics of the Micelles at α ~ 0.9−1.0 and 0.1 M Added NaCl[a]

	$N_{agg,SLS}$	$R_{c,SLS}$[b] (nm)	$R_{c,SANS}$ (nm)	$N_{agg,SANS}$[c]	$R_{c,TEM}$ (nm)	d_{corona}[d] (nm)	stretching of PAA[e] (%)
P*n*BA$_{90}$−PAA$_{100}$	440	12.5	11.3	330	11.5 ± 0.5	21	84
P*n*BA$_{100}$−PAA$_{150}$	370	12.2	9.7	189		34	90
P*n*BA$_{90}$−PAA$_{300}$	270	10.6	9.7	208	9.0 ± 0.5	46	62

[a] The SANS and cryo-TEM results were obtained at α = 1.0 and 0.1 M added NaCl. [b] Calculated from N_{agg} according to eq 6. [c] Calculated from R_c according to eq 6. [d] $d_{corona} = R_h - R_{c,SANS}$. [e] $d_{corona}/L_{contour,PAA}$.

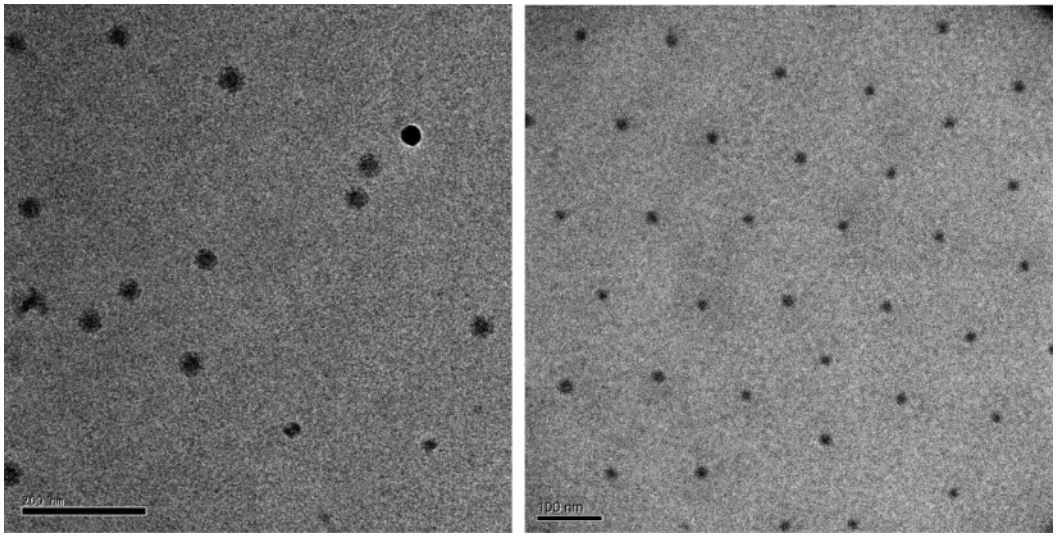

Figure 2. Cryo-TEM images of P*n*BA$_{90}$−PAA$_{100}$ (left) and P*n*BA$_{90}$−PAA$_{300}$ (right) at 0.5 g/L, pH ∼ 10 (α = 1), and 0.1 M NaCl. The scale bar corresponds to 200 nm in the left image and 100 nm on the right one. The black dot is an ice crystal.

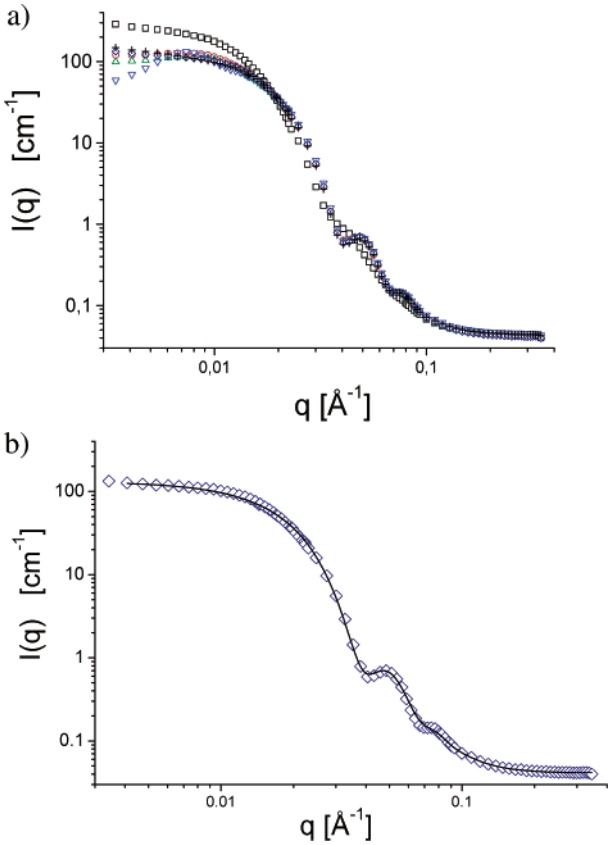

Figure 3. (a) SANS curves for 10 g/L samples of P*n*BA$_{90}$−PAA$_{100}$ in D_2O for various amounts of added NaCl and degrees of ionization, α: (□) α = 0.2, 0.1 M NaCl; (○) α = 0.5, 0.1 M NaCl; (△) α = 1.0, 0.1 M NaCl; (▽) α = 1.0, 0.01 M NaCl; (◇) α = 1.0, 0.5 M NaCl; (+) α = 1.0, 1.0 M NaCl. (b) SANS scattering curve for the sample of P*n*BA$_{90}$−PAA$_{100}$ at α = 1.0 and 0.5 M NaCl (◇) including a fit.

salt at this α value has indeed hardly any influence on the scattering curves for $q > 0.02$ Å^{-1}. Thus, it is obvious that the structure of the micelles is not affected by the change of ionic strength.

However, it is interesting to note that in the low q range of the SANS experiments, which is dominated by the structure factor, $S(q)$, i.e., the interactions between the micellar aggregates, pronounced differences between the three polymers are observed (Figures 3−5). While P*n*BA$_{90}$−PAA$_{100}$ shows only a weakly

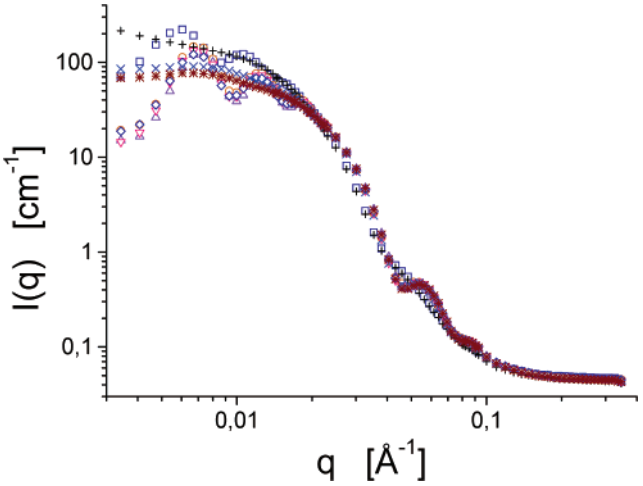

Figure 4. SANS curves for 10 g/L samples of P*n*BA$_{100}$−PAA$_{150}$ in D_2O for various amounts of added NaCl and degrees of ionization α: (□) α = 0.2, 0 M NaCl; (○) α = 0.5, 0 M NaCl; (△) α = 0.75, 0.1 M NaCl; (▽) α = 0.9, 0 M NaCl; (◇) α = 1.0, 0 M NaCl; (+) α = 0.2, 0.1 M NaCl; (×) α = 0.5, 0.1 M NaCl; (*) α = 1.0, 0.1 M NaCl.

pronounced $S(q)$ peak at low ionic strength, the situation is completely different for the P*n*BA$_{100}$−PAA$_{150}$ and P*n*BA$_{90}$−PAA$_{300}$ micelles. Here, a very pronounced peak with higher orders (up to a third-order maximum, Figures 4 and 5) is observed and vanishes only for the highest salt concentrations. This strong electrostatic interaction for the system with longer PAA block is very interesting as such an effect has not been observed for similarly constructed diblock copolymer micelles of the PIB−PMAA type in the same concentration range. However, the persistence of the correlation peak up to 0.1 M NaCl for P*n*BA$_{100}$−PAA$_{150}$ and 1 M for P*n*BA$_{90}$−PAA$_{300}$ may be due to the high concentration of polymer necessary to get a high signal-to-noise ratio in the SANS experiments. From the position of the correlation peak one can calculate the mean spacing between the aggregates via the relation $d = 2\pi/q_{max}$, leading to values from 85 to 110 nm for all polymer solutions. Consequently, the coronas of the micelles formed by P*n*BA$_{90}$−PAA$_{300}$ at 0.1 M of NaCl already touch each other (R_h > 50 nm, Table 3) at this polymer concentration and stretched chains of PAA would already largely overlap. However, apparently such an overlapping is not yet strongly taking place as one still observes a pronounced correlation peak that indicates strong

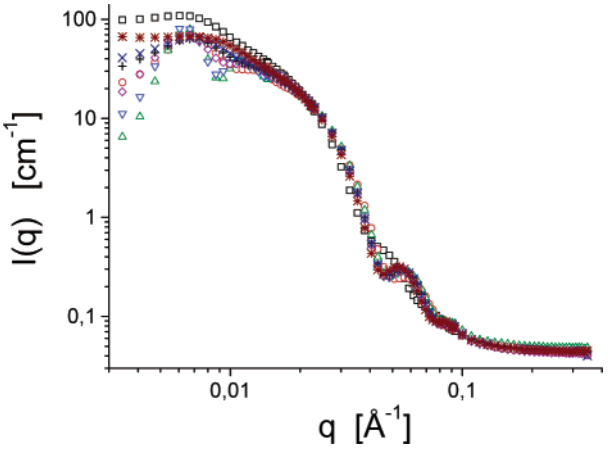

Figure 5. SANS curves for 10 g/L samples of P*n*BA$_{90}$−PAA$_{300}$ in D_2O for various amounts of added NaCl and degrees of ionization α: (□) α = 0.2, 0.1 M NaCl; (○) α = 0.5, 0.1 M NaCl; (△) α = 1.0, 0 M NaCl; (▽) α = 1.0, 0.01 M NaCl; (◇) α = 1.0, 0.1 M NaCl; (+) α = 1.0, 0.3 M NaCl; (×) α = 1.0, 0.5 M NaCl; (*) α = 1.0, 1.0 M NaCl.

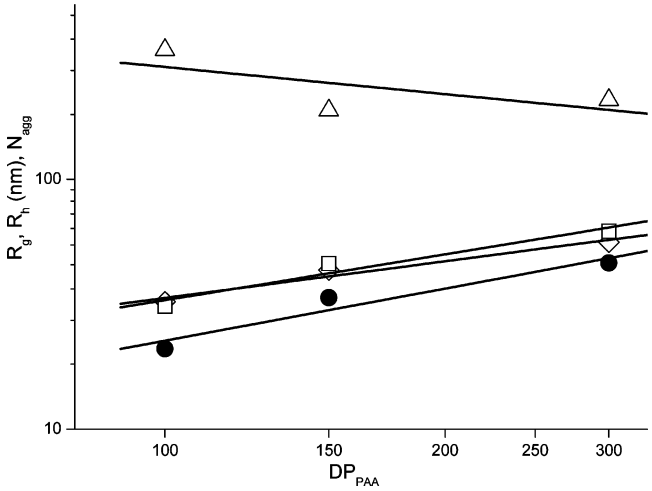

Figure 6. Effect of the PAA block length on the characteristics of the micelles formed by the block copolymers at (α ∼ 0.9−1) and 0.1 M NaCl: R_h (◇), R_g (□), $N_{agg,SANS}$ (△), d_{corona} (●).

interactions in spite of the very short screening length of the solution (1 nm in a 0.1 M NaCl solution and 0.32 nm in a 1 M NaCl solution). At higher salt concentration, or with shorter PAA blocks, the hydrodynamic radius of the micelles decreases (Table 3), and the aggregates are separated by a sufficient distance to allow electrostatic interactions to be screened efficiently.

The fact that strong intermicellar repulsions exist between the micelles in the absence of added salt is confirmed by DLS (Figure 8). Indeed, Figure 8a shows that the apparent hydrodynamic radius $R_{h,app}$ strongly depends on the magnitude of the scattering vector in the absence of added salt. This behavior could arise from different reasons: anisotropy, high polydispersity, or strongly pronounced static and hydrodynamic interactions, i.e., the impact of the hydrodynamic structure factor, $H(q)$, and the static structure factor, $S(q)$, on the apparent radii obtained by DLS: $R_{h,app} = R_{h,0}H(q)/S(q)$. Cryo-TEM, SANS, and DLS clearly proved the presence of spherical particles with low polydispersity. (Cumulant treatment of the DLS data reveals a polydispersity $p = \mu^2/\Gamma^2 \sim 0.1$.) As a consequence, the dependence of the apparent R_h on q^2 for P*n*BA$_{90}$−PAA$_{300}$ (and similarly for P*n*BA$_{90}$−PAA$_{100}$) in the absence of added salt is likely the result of intermicellar interactions. Note that the polymer concentration used for DLS (0.5 g/L) is low enough to allow micelles to be well separated from each other. Thus, the strong interactions between the micelles are truly caused by electrostatic interactions.

The significant decrease of micelles' hydrodynamic radii with increasing salt concentration, which was also observed by FCS,[1] can be entirely attributed to the contraction of the PAA corona by the increase of ionic strength, as the core radius, R_c, remains constant for all polymers between 0 and 1 M NaCl (Table 3). The repulsive electrostatic interactions between negatively charged PAA chains become more and more screened when the salt concentration increases. Although the effect is not as strongly pronounced for P*n*BA$_{90}$−PAA$_{100}$, it can still be observed: R_h decreases steadily from 33 to 26 nm from 0.005 M added NaCl to 1 M NaCl. (The point without added NaCl should be disregarded since R_h depends slightly on q^2 for this point.)

3. Effect of the Degree of Ionization. The behavior of P*n*BA$_{90}$−PAA$_{300}$ at different pH was also studied by DLS, SLS, SANS, and cryo-TEM at a constant salt concentration of 0.1 M NaCl. All solutions were prepared by dissolution method 1. However, since the polymer does not dissolve spontaneously for α < 0.2, the solution at pH = 2.9 (α ∼ 0) was obtained by

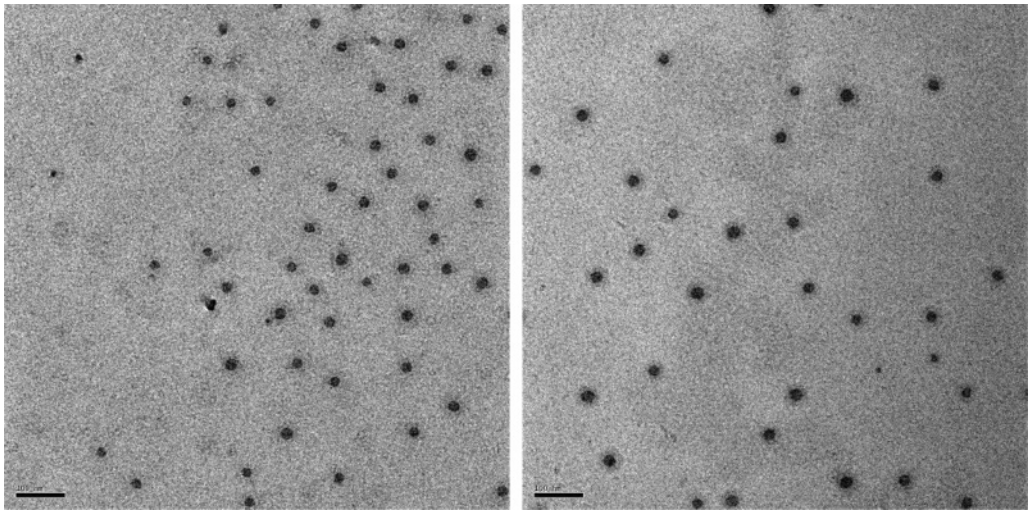

Figure 7. Cryo-TEM at 0.5 g/L and pH ∼ 10 (α = 1) of P*n*BA$_{90}$−PAA$_{100}$ at 0.01 M NaCl prepared using method 1 (left) and without added salt (right). The scale bar corresponds to 100 nm.

Table 3. Effect of the NaCl Concentration on the Characteristics of Micelles of P*n*BA$_{90}$−PAA$_{100}$ and P*n*BA$_{90}$−PAA$_{300}$ at pH 9−11 (α ∼ 1)

	[NaCl] (mol/L)	R_h (nm)	$R_{c,TEM}$ (nm)	$N_{agg,TEM}$	$R_{c,SANS}$ (nm)	$N_{agg,SANS}$	d_{corona} (nm)	stretching of PAA (%)
P*n*BA$_{90}$−PAA$_{100}$	0[a]	30	12 ± 0.5	400 ± 50			18	72
	0.005	33					21	86
	0.01	32	12 ± 0.5	400 ± 50	11.2	303	21	85
	0.1	30	11.5 ± 0.5	400 ± 50	11.3	330	19	75
	0.5				11.3	337		
	1.0	26			11.3	331	14	57
P*n*BA$_{100}$−PAA$_{150}$	0.0[a]				9.6	192		
	0.1	43[b]			9.7	205	34	90
P*n*BA$_{90}$−PAA$_{300}$	0.0[a]	61			9.4	186		
	0.01	61			9.6	200	52	69
	0.1	51	9 ± 0.5	170 ± 30	9.7	208	42	55
	0.3				9.7	205		
	0.5				9.8	216		
	1.0	42			9.7	210	32	43

[a] Because of addition of NaOH, the ionic strength corresponds to a salt concentration of 2.7, 3.2, and 4.5 mM for P*n*BA$_{90}$−PAA$_{100}$, P*n*BA$_{100}$−PAA$_{150}$, and P*n*BA$_{90}$−PAA$_{300}$, respectively. [b] Obtained at α ∼ 0.9.

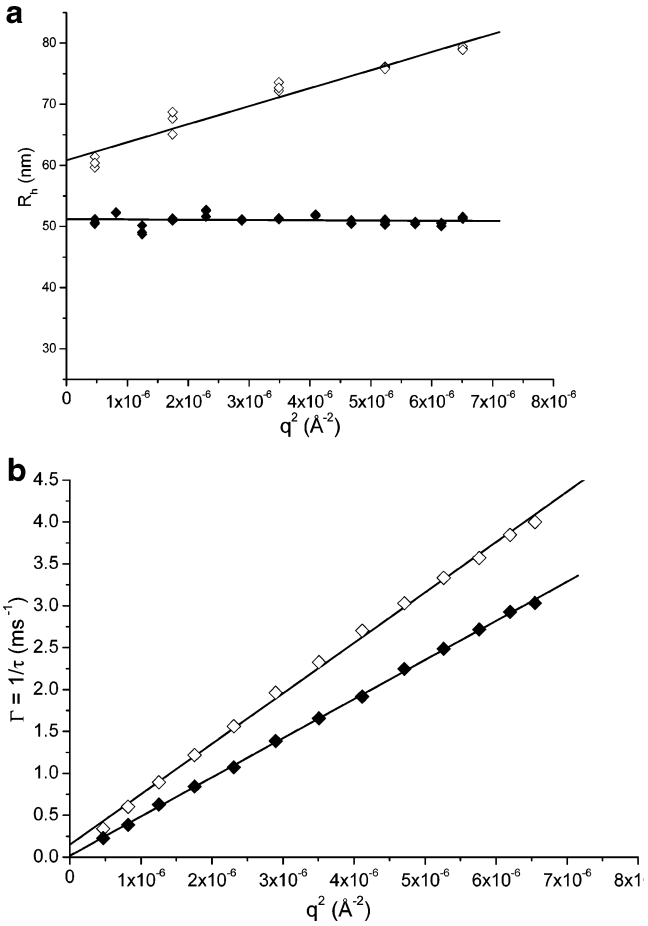

Figure 8. (a) Evolution of the hydrodynamic radius and (b) of the rate constant, Γ, for P*n*BA$_{90}$−PAA$_{300}$ at c = 0.5 g/L and pH ∼ 11 (α = 1). The legend is the same for both figures: (◇) without added salt, (◆) with 0.1 M NaCl.

dissolving the polymer at pH > 8 (α ∼ 1) in pure water and then adjusting the pH and salt concentration after dissolution of the polymer. SLS was again performed with dialyzed solutions having a polymer concentration ranging from 0.2 to 2.0 g/L, whereas DLS and cryo-TEM were conducted at a polymer concentration of 0.5 g/L. For SANS experiments (Figure 5), polymer solutions at 10 g/L having a degree of ionization α between 0.2 and 1.0 and containing 0.1 M NaCl were used.

All experiments (see Figure 5 and Table 4) indicate that the R_h, R_g, and N_{agg} of the aggregates do not change significantly from pH ∼ 10 (α = 1) down to pH ∼ 5.5 (α ∼ 0.5). Moreover, at pH ≥ 5.5, the apparent R_h is rather independent of the scattering angle, and the SANS curves do not change significantly, indicating that spherical micelles of rather low polydispersity, p = 0.12 (R_{c-SANS}) and p ∼ 0.1 (R_h), are obtained.

The characteristics of the aggregates obtained at pH < 5.5 are strongly different. Cryo-TEM reveals the presence of spherical micelles at 0.1 M NaCl for pH ∼ 3.5 (Figure 9) as well as for pH ∼ 11 (Figure 2, right). However, the micelles have a clear tendency for clustering at low pH, whereas they are randomly dispersed at higher pH. The formation of clusters of micelles is confirmed by DLS, where bimodal or very broad distributions of R_h are observed (data not shown). In addition, the apparent R_h, estimated by considering the whole broad distribution, becomes strongly dependent on the scattering angle (see Figure 11), an indication for strong intermicellar interactions, as noted above. Moreover, the respective SANS scattering curves look clearly different at α = 0.2, as compared to α = 0.5 or 1. The characteristic minimum at q = 0.04−0.05 Å, indicating the monodispersity of spherical particles, is not present at the lowest α value. Furthermore, one notices an increase in scattering intensity at low q that is indicative of attractive interactions between the particles and the concomitant formation of micellar clusters. Finally, the strong influence of the structure factor, caused by attractive interactions, is also evident in a highly pronounced nonlinear q dependence of the SLS data (Figure 10). A meaningful data treatment by extrapolations according to Zimm was not possible. As a consequence, neither the SLS nor the DLS data were quantitatively treated at low pH.

From the SANS data it is apparent that the mean size of the core of the individual micelles increases markedly when going from α ≥ 0.5 to α ∼ 0.2. In that context, it must be noted that the SANS data at α ∼ 0.2 and 0.1 M NaCl could only be treated successfully by assuming that a part of the protonated PAA block collapses in a dense shell around the P*n*BA core. This can be deduced from the fact that the scattering intensity increases more than would be expected simply on the basis of an increase in size of the aggregates for a constant volume fraction of core material (see eqs 2 and 3). Accordingly, the additional increase has to be due to an additional scattering mass that must come from the now less charged corona. This is a plausible scenario as the uncharged PAA is much less hydrophilic than the deprotonated one. However, its detailed location within the aggregate would only be deduced from more detailed structural investigations, e.g., a SANS contrast variation employing deuterated PAA. Prochazka et al. already found that

Table 4. Effect of pH on the Characteristics of the Micelles of P*n*BA$_{90}$−PAA$_{300}$ at 0.1 M NaCl

pH	α	$N_{agg,SLS}$	$R_{c,SLS}$ (nm)	$R_{g,SLS}$ (nm)	10^6A_2 (mol mL/g^2)	$R_{h,DLS}$ (nm)	$R_{c,TEM}$ (nm)	$N_{agg,TEM}$	$R_{c,SANS}$ (nm)	p^c	$N_{agg,SANS}$	d_{corona} (nm)	stretching of PAA (%)	X^d (%)
11−12	1.0	310	11.1	67	35	51	9 ± 0.5	165 ± 35	9.7	0.12	208	42	55	0
7.3	0.90	270	10.6	65	43	56						46	62	
6.5	0.75	240	10.2	54	47	51								
5.5	0.50	280	10.7	61	43	51			9.1	0.14	159	42	56	4
4.7	0.25	*a*	*a*	*a*	*a*	*a*								
	0.20								10.3	0.21	180			21
2.9	0.0	*a*	*a*	*a*	*a*	*a*	18 ± 0.5[b]	1300 ± 100[b]				*a*	*a*	

[a] The DLS and SLS data are strongly influenced by the clustering of micelles at low pH and could not be treated quantitatively for this reason. [b] Under these conditions the protonated PAA block is partially collapsed at the core−corona interface (see SANS at α = 0.2 and corresponding description in the text). [c] Polydispersity index. [d] X = apparent fraction of PAA in the core.

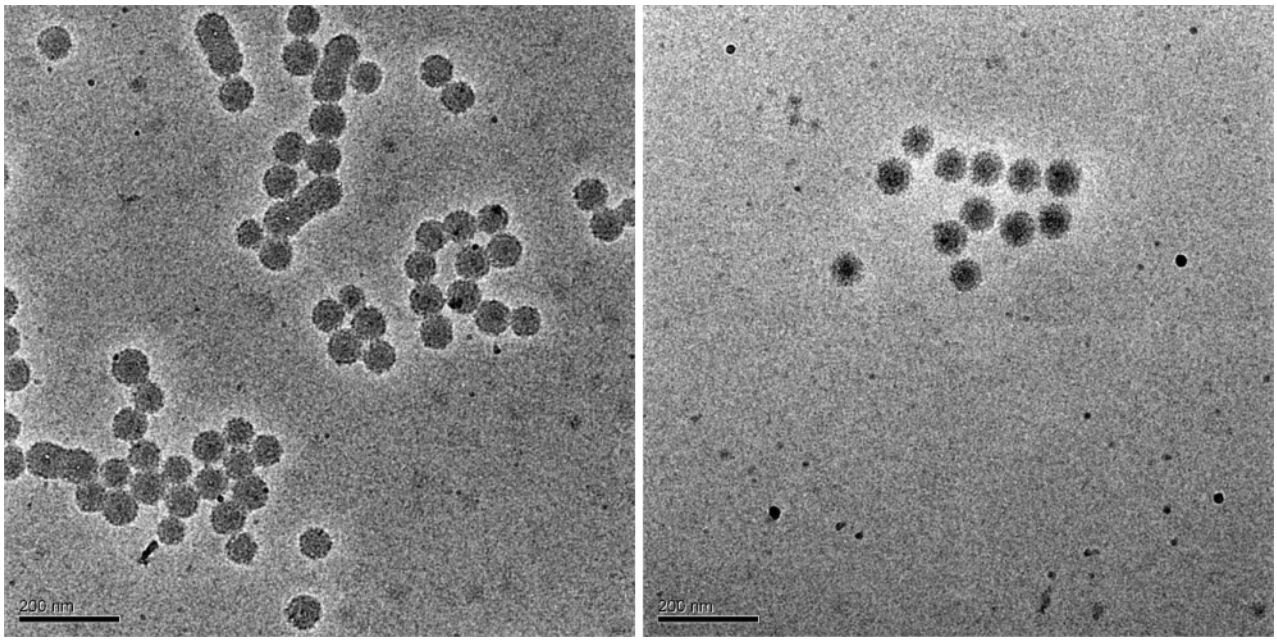

Figure 9. Cryo-TEM at 0.5 g/L, pH ∼ 3.5 (α ∼ 0) of P*n*BA$_{90}$−PAA$_{300}$ at 0.1 M NaCl prepared using method 1. The scale bar corresponds to 200 nm. Whereas the left picture more strikingly reflects the clustering of micelles, the contrast is better in the right picture, enabling to see both the core and the dense part of the corona of the micelles. Both pictures were however obtained with the same polymer solution and the apparent difference of concentration or contrast is an artifact of the cryo-TEM method.

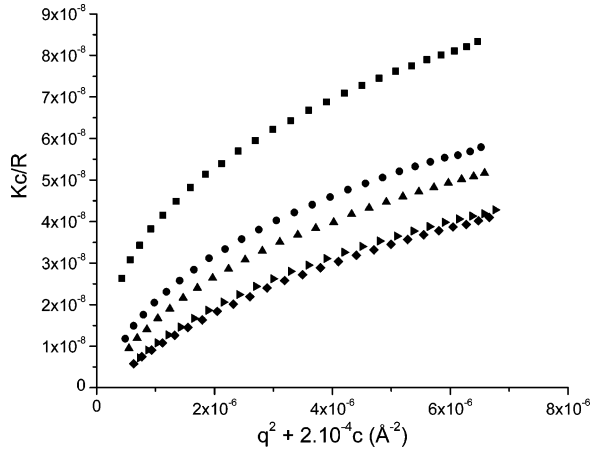

Figure 10. Zimm plot of P*n*BA$_{90}$−PAA$_{300}$ at pH ∼ 3 (α = 0) and 0.1 M NaCl. c = 0.5 (■), 0.8 (●), 1.1 (▲), 1.5 (◆), and 2.0 g/L (tilted ▲) of polymer.

part of the PMAA corona of PS−PMAA micelles forms a dense shell around the polystyrene core; however, such a phenomenon has not been reported for the more hydrophilic PAA.[3,16−21]

The size of the hydrophobic core, and thus N_{agg}, seems to increase dramatically at pH = 2.9 (α = 0) according to cryo-TEM (Figure 9, Table 4). However, the dimensions of the denser part of the micelles (that is the whole core surrounded by a part of the corona only) do not seem to change significantly even at this pH as $R_{micelle}$ changes from 37 ± 2 nm at pH ∼ 7 to 33 ± 2 nm at pH ∼ 3.5. It is however possible that the darkest part of the P*n*BA$_{90}$−PAA$_{300}$ micelles at pH = 2.9 and 0.1 M NaCl is composed of a dense P*n*BA core surrounded by a dense, partially collapsed PAA shell as observed at α ∼ 0.2 by SANS. Consequently, we are not sure that N_{agg} increases that significantly at pH = 2.9.

In conclusion, the size of individual micelles is not significantly influenced by pH for pH ≥ 5.5, and N_{agg} remains constant even down to pH = 4.7 (at this pH, no information on R_h could be obtained from DLS). The increase of N_{agg} estimated from $R_{c,TEM}$ at pH = 2.9 (α = 0) is apparent only, since the P*n*BA core observed by cryo-TEM at this pH is surrounded by a dense shell of partially collapsed PAA. In addition, light scattering, cryo-TEM, and SANS indicate the clustering of micelles at pH ≤ 4.7 (α ≤ 0.25). We interpret this phenomenon as being due to the formation of intermicellar hydrogen bonds between the protonated AA units of the hydrophilic block at low pH and to the fact that the PAA corona is less hydrophilic in the protonated state. The clustering of micelles at pH ≤ 4.7 is consistent with the fact that the polymers are not spontaneously soluble below this pH. A scattering angle dependence of R_h was also observed at 0.01 M NaCl and pH < 5.5 for P*n*BA$_{90}$−PAA$_{300}$ at 0.5 g/L.

Table 5. Effect of Ionization Degree, α, on the Characteristics of the Micelles Determined by SANS (for P*n*BA$_{90}$−PAA$_{300}$, See Table 4)

	[NaCl] (M)	α	$R_{c,SANS}$ (nm)	p	$N_{agg,SANS}$	fraction of collapsed PAA at core−corona interface (%)
P*n*BA$_{90}$−PAA$_{100}$	0.1	1	11.2	0.13	317	0
	0.1	0.5	11.3	0.13	321	4
	0.1	0.2	13.2	0.20	378	59
P*n*BA$_{100}$−PAA$_{150}$	0.1	1	9.7	0.13	189	0
	0.1	0.5	10	0.15	197	7
	0.1	0.2	11.2	0.23	203	55
	0	1	9.5	0.13	180	0
	0	0.9	9.8	0.13	192	0
	0	0.75	9.7	0.13	190	2
	0	0.5	10	0.14	193	7
	0	0.2	10.9	0.21	194	45

The clustering of micelles at low pH thus also occurs at low ionic strength.

Although only SANS analyses were performed to investigate the effect of pH on the nature of micelles formed by the other two block copolymers, P*n*BA$_{90}$−PAA$_{100}$ and P*n*BA$_{100}$−PAA$_{150}$ (Figures 3a and 4, Tables 4 and 5), the same conclusions as for P*n*BA$_{90}$−PAA$_{300}$ can be drawn.

In order to see whether the clustering of micelles at low pH is reversible, various pH jumps between pH ∼ 8−10 (α ∼ 1) and pH ∼ 3.5 (α ∼ 0) were performed in a cyclic manner. P*n*BA$_{90}$−PAA$_{300}$ was first dissolved at pH ∼ 10 and then brought to 0.1 M NaCl (method 1). The pH was then changed four times, i.e., through two cycles (α ∼ 1 → ∼0 → ∼1 → ∼0 → ∼ 1) by quickly adding either 0.4 M HCl or 2 M NaOH. After one night of stirring following each pH change, the solutions were measured by DLS. Under those conditions, the polymer concentration hardly changed (0.5 g/L ± 2%), whereas the salt concentration slightly increased to 0.12 M after four pH changes.

As can be seen in Figure 11, the apparent R_h of the micelles at pH > 8 is initially independent of the scattering angle. It increases from R_h ∼ 50 nm to R_h > 100 nm after several pH changes, while its angular dependence becomes stronger. In contrast, at pH < 3.5, the initially strong angular dependence decreases with the number of cycles, but R_h at 90° increases. These observations most probably indicate that the clusters of micelles formed at low pH only partially dissociate overnight upon pH change and thus that the cluster formation and destruction are governed by slow dynamics in the range of days. Longer equilibration periods between each pH change might have permitted complete separation of the aggregates, but we will see below that weeks might have been required.

4. Effect of the Method of Preparation of the Polymer Solution on the Micellar Structure. Polymer solutions characterized so far were prepared by first dissolving the polymer in water without added salt at the desired α, followed by adding salt after at least one night of equilibration (method 1). In this section, we will compare this method of preparation with method 2, where the polymer solution is prepared in one step by dissolving the polymer directly in an aqueous salt solution at the desired salt concentration and pH. Two solutions of P*n*BA$_{90}$−PAA$_{300}$ at 2.0 g/L were prepared at pH ∼ 6.5 (α ∼ 0.75) and 0.1 M NaCl, using either method 1 or method 2. These stock solutions were then dialyzed against water at the same pH and 0.1 M NaCl, and then diluted with the dialyzate, finally furnishing solutions ranging from 0.2 to 2.0 g/L that were used for SLS experiments. The solutions at 0.5 g/L were also exploited for DLS and cryo-TEM.

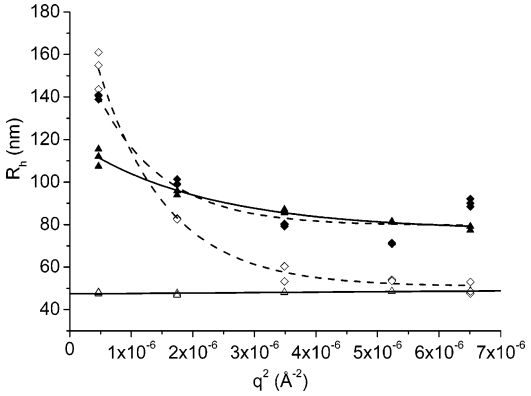

Figure 11. Effect of pH cycles on the scattering vector dependence of R_h for P*n*BA$_{90}$−PAA$_{300}$ with 0.1 M NaCl: (△) pH ∼ 8 (α ∼ 1, start), (◇) pH ∼ 3.5 (α ∼ 0, first pH jump), (◆) pH ∼ 3.5 (α ∼ 0, third pH jump), (▲) pH ∼ 8 (α ∼ 1, fourth pH jump). The second pH jump (back to pH ∼ 8) is not shown for clarity since it is similar to the fourth pH jump with a less pronounced R_h dependence.

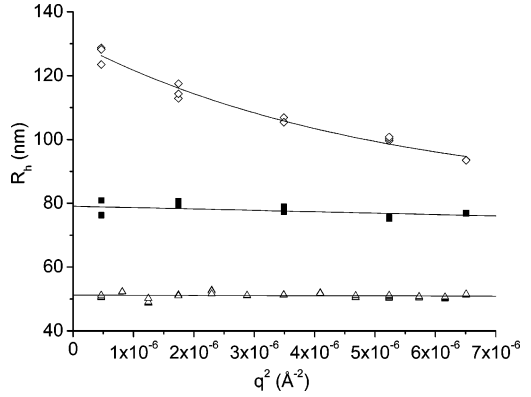

Figure 12. Effect of the sample preparation method on the scattering vector dependence of R_h for P*n*BA$_{90}$−PAA$_{300}$ for α ∼ 1 with 0.1 M NaCl: (◇) method 2, 1 day after the preparation of the solution; (■) method 2, 3 months after the preparation of the solution; (△) method 1, 1 day after the preparation of the solution.

It has first to be highlighted that particles obtained by both preparation methods described above are of spherical shape (Figure 13). The sample prepared with method 2 was not analyzed directly by cryo-TEM, but 1 month after its preparation. However, the shape of the particles should not have evolved significantly within this period, as will be discussed below.

The other characteristics of the particles obtained with both methods of preparation are highly different. First, the spherical micelles obtained with method 1 are monodisperse, randomly distributed (Figures 12−14) and do not change with time, as already discussed in the previous sections. On the contrary, the micelles obtained shortly after the dissolution of the polymer using method 2 tend to aggregate into clusters of micelles. This conclusion is supported by DLS. Indeed, the apparent R_h strongly depends on the scattering angle a few days after the preparation of the solution using method 2 (Figure 12). As stated in the previous sections, the dependence of R_h on the scattering vector is most likely attributed to strong intermicellar interactions (cf. section 2). The curvature of the SLS Zimm plot (Figure 14, right) also reveals strong intermicellar interactions. Finally, although the cryo-TEM image was obtained 1 month after the preparation of the solution (Figure 13b), it still indicates that the micelles are not randomly distributed, but rather grouped into clusters. Qualitatively, the formation of clusters of micelles was also observed by means of cryo-TEM, SLS, and DLS, when

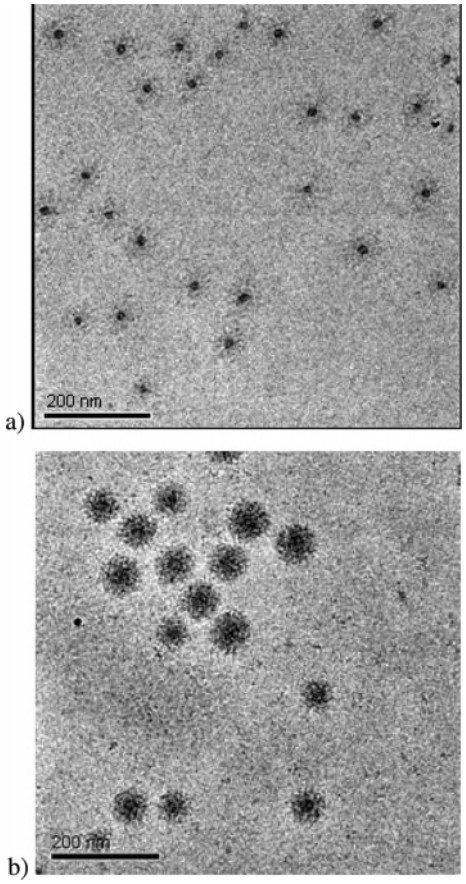

Figure 13. Cryo-TEM at pH ~ 6.4 (α ~ 0.75) of P*n*BA$_{90}$−PAA$_{300}$ prepared with 0.1 M NaCl using (a) method 1 and (b) method 2. Scale bar = 200 nm.

P*n*BA$_{90}$−PAA$_{100}$ was directly dissolved at pH ~ 10 (α = 1) in a Na_2CO_3/$NaHCO_3$ (0.05 M/0.05 M) buffer.

In order to further discuss the differences between the micelles obtained with either method, quantitative treatment of the DLS, SLS, and cryo-TEM data would be required. However, the strong intermicellar interactions present in the system prepared according to method 2 initially prevent any quantitative treatment of the DLS and SLS data. Cryo-TEM could have been used to obtain quantitative information on the size of the core. However, these experiments were made 1 month after the preparation of the solution, and we did not know at this point whether the solutions changed during this period.

Thus, we investigated the evolution with time of a solution prepared with method 2: P*n*BA$_{90}$−PAA$_{300}$ was dissolved at 0.5 g/L, in an aqueous solution of 0.1 M NaCl at pH = 10. The evolution of the apparent R_h with time was monitored by DLS. As can be observed in Figure 15, the hydrodynamic radius of the particles decreases very slowly, reaching a plateau after about 1 month. On the plateau, the initial scattering angle dependence of R_h has disappeared, which probably points to a breakup of the initial micelle clusters into rather monodisperse and randomly distributed spherical micelles. After this time, no further evolution is indicated. Noteworthy, the micelles finally obtained with method 2 are much larger (R_h ~ 80 nm) than those obtained with method 1 (R_h ~ 50 nm, see Table 6). Even their aggregation number differs, as supported by the cryo-TEM imaging on these micellar solutions (vide supra). This may be explained by the efficient screening of charges of the PAA segment in the presence of salt which reduces their intermolecular repulsion and facilitates the incorporation of more chains per micelle. As a consequence, the initial apparent aggregation number is larger (compared to method 1), which is accompanied by a stronger stretching of the corona (Table 6). The fast aggregation and the effective screening of repulsive interactions between those big micelles may also be responsible for the formation of thermodynamically unstable clusters of micelles, which slowly disintegrate with time.

Thus, it is obvious that micelle formation strongly depends on the preparation conditions, indicating a kinetic control of micelle formation, as will be discussed below.

Conclusions

Our experiments with P*n*BA−PAA amphiphilic block copolymers have brought about some unexpected results, which—at first glance—may appear to be contradictory:

(i) The polymers readily self-assemble into spherical micelles with low dispersity in aqueous media when dissolved under salt-free basic conditions without the need of any cosolvent, typical for dynamic micelles.

(ii) Dissolving the polymer in the presence of added salt leads to the formation of larger particles with a strong tendency for cluster formation. In addition, the hydrodynamic radii, the aggregation numbers (see Table 6), and the polydispersities of micelles obtained in saline solution slowly decrease with time. Furthermore, the final size of the micelles, which is correlated with the aggregation numbers at a given pH and ionic strength, is strongly dependent on the initial preparation conditions. Micelles self-assembled in saline solutions are significantly larger than micelles obtained in the absence of added salt.

(iii) The micellar size (in terms of the thickness of the charged corona) may be tuned by pH and salinity, as expected for micelles comprising a weak polyelectrolyte shell.

(iv) The FCS studies presented in our earlier paper[1] show the existence of a (very low) "apparent" cmc and a decrease of the hydrodynamic radius of the micelles in the absence of added salt upon dilution, whereas it stays constant in saline media.

(v) However, neither light scattering, nor neutron scattering, nor cryo-TEM provides any significant evidence for structural rearrangements with respect to aggregation number and morphology upon these external stimuli, which is typical for "frozen" micelles.

We already interpreted the FCS results in terms of the nucleation theory of micellization according to the closed association model,[22−25] which predicts that micellization of block copolymers with a lyophobic soft block (low T_g) are dynamic in nature by exchanging unimers but do not reach thermodynamic equilibrium within the experimental time window. We believe that this model is also able to explain the results presented in this paper.

Obviously, the kinetics of unimer exchange is slower in the presence of added salt. As was outlined before,[1] this can be attributed to the less hydrophilic nature of the PAA shell when charges are screened. Unimers are more easily expelled from micelles via Coulomb repulsion in salt-free solution, whereas they undergo hydrophobic attraction in a screened corona.

Therefore, we regard the system to be dynamic with respect to unimer exchange. This interpretation is well in line with recent results by Garnier and Laschewsky.[26] They reported mixing experiments of diblock copolymer micellar aggregates composed of a P*n*BA block (DP_{PnBA} = 37−95) and various hydrophilic blocks, such as poly(*N*,*N*-dimethylacrylamide) (PDMAAm) and poly(3-acrylamidopropyltrimethylammonium chloride) (PAPTA). Mixing pure micelles of P*n*BA$_{37}$−PDMAAm$_{70}$ (R_h = 12.5 nm) and P*n*BA$_{81}$−PAPTA$_{105}$ (R_h = 134 nm) resulted in mixed micelles of 96 nm after 3 days. These experiments

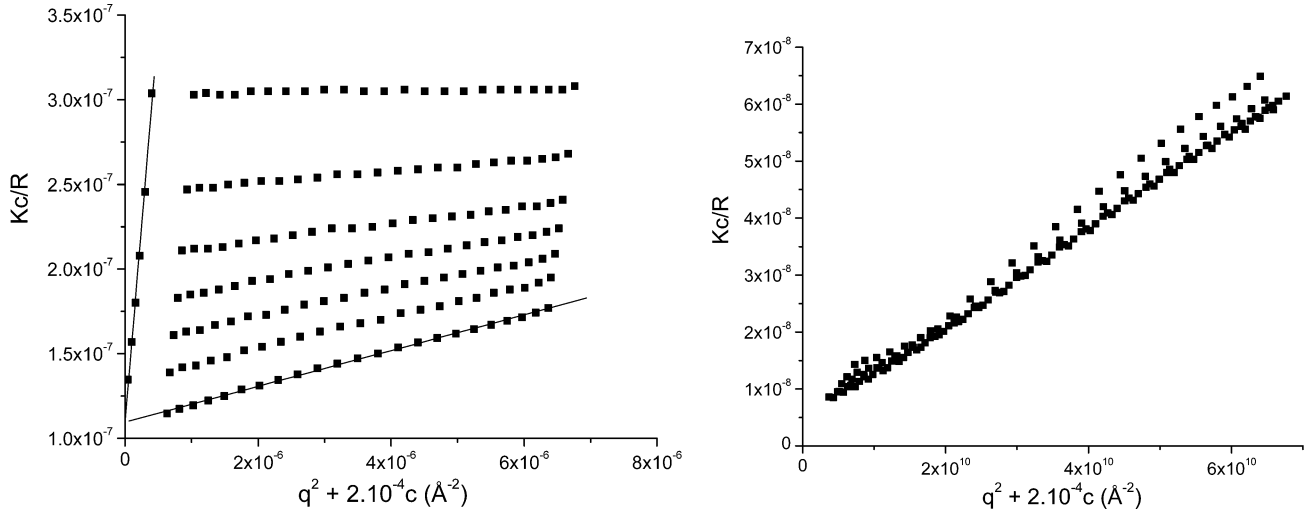

Figure 14. Zimm plot of P*n*BA$_{90}$−PAA$_{300}$ (c = 0.2−2 g/L) at pH ∼ 6.4 (α ∼ 0.75) and 0.1 M NaCl: left, method 1; right, method 2.

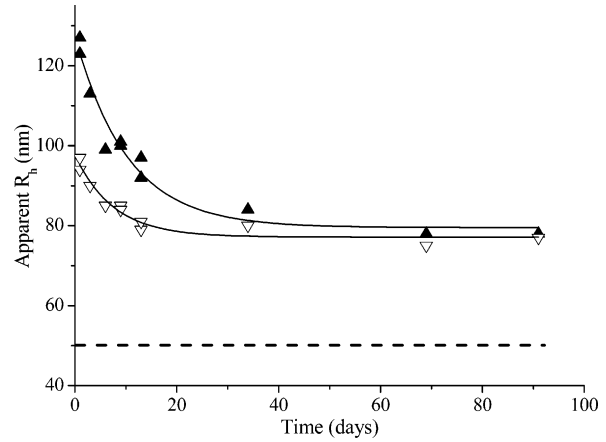

Figure 15. Evolution of the apparent hydrodynamic radius at 30° (▲) and 150° (▽) with the time of stirring at room temperature for a solution of P*n*BA$_{90}$−PAA$_{300}$ prepared using method 2 at pH ∼ 10 and 0.1 M NaCl. The continuous lines represent exponential fits of the experimental points. The dashed straight line represents the hydrodynamic radius of a solution prepared in the same conditions but with method 1.

Table 6. Characteristics of the Micelles of P*n*BA$_{90}$−PAA$_{300}$ Depending on the Preparation Method at α ∼ 0.75 and 0.1 M NaCl

	pH	R_h (nm)	R_c (nm)	N_{agg}	d_{corona} (nm)	stretching of PAA (%)
method 1	6.5	50	8.5 ± 0.5	140 ± 26	42	56
method 2[a]	6.3	80	14.5 ± 0.5	695 ± 75	65	87

[a] For method 2, the characteristics were evaluated at least 1 month after the preparation of the solution to allow for the destruction of the micellar clusters.

indicate that unimer exchange between the micelles is occurring with P*n*BA blocks of similar length as ours. They also prove the slow kinetics involved in unimer exchange dynamics of amphiphilic block copolymers.

As highlighted above, the sizes and the aggregation numbers (see Table 6) strongly depend on the salinity during preparation of the micellar solutions and therefore on the initial preparation conditions. This is in agreement with what was reported by Martin et al.[27] for micelles consisting of poly(vinylpyridine)-*b*-poly(ethylene oxide). The corresponding micellar sizes were shown to be strongly dependent on the initial polymer concentration.

Mizellization of P*n*BA−PAA arises therefore as a kinetically controlled process in accordance with theory of Nyrkova and Semenov.[25] Consequently, a change of the aggregation number or any further structural rearrangement upon external stimuli may be prohibited within the experimental time window as long as the reduced interfacial energy of the core−shell vicinity is high enough. Considering our presented experimental results, this is indeed evident in our system. This argumentation may also apply for micelles observed by Martin et al. Here, too, the micellar sizes depend neither on pH nor on formation rate.[24,27] Furthermore, this interpretation is sustained by experimental results obtained with PIB$_{75}$-*b*-PMAA$_{190}$ block copolymers.[6] These block copolymers are comparable to our polymers in terms of hydrophobic and hydrophilic block lengths but obviously have a lower interfacial energy between both blocks than in the case of P*n*BA−PAA, thus allowing for structural changes within the experimental time window upon external stimuli.

Acknowledgment. This work was supported by the European Union within the Marie Curie RTN Polyamphi and by DFG within the ESF EUROCORES Programme SONS. We thank Karlheinz Lauterbach for the determination of d*n*/d*c* and Oleg Borisov, Laurent Bouteiller, Christophe Chassenieux, and Mingfu Zhang for helpful discussions. ILL is gratefully acknowledged for providing SANS beam time and travel support.

References and Notes

(1) Colombani, O.; Ruppel, M.; Schubert, F.; Zettl, H.; Pergushov, D. V.; Müller, A. H. E. *Macromolecules* **2007**, *40*, 4338−4350.
(2) Zhang, L.; Barlow, R. J.; Eisenberg, A. *Macromolecules* **1995**, *28*, 6055−6066.
(3) Förster, S.; Hermsdorf, N.; Bottcher, C.; Lindner, P. *Macromolecules* **2002**, *35*, 4096−4105.
(4) Förster, S.; Abetz, V.; Müller, A. H. E. *Adv. Polym. Sci.* **2004**, *166*, 173−210.
(5) Förster, S.; Hermsdorf, N.; Leube, W.; Schnablegger, H.; Regenbrecht, M.; Akari, S.; Lindner, P.; Böttcher, C. *J. Phys. Chem. B* **1999**, *103*, 6657−6668.
(6) Burkhardt, M.; Ruppel, M.; Martínez-Castro, N.; Tea, S.; Pergushov, D. V.; Gradzielski, M.; Müller, A. H. E. Dynamic Phenomena in aqueous PIB$_X$-b-PMAA$_Y$ Micellar and IPEC solutions. Poster Presentation: 6th International Symposium on Polyelectrolytes, Dresden, 2006.
(7) Pergushov, D. V.; Remizova, E. V.; Gradzielski, M.; Lindner, P.; Feldthusen, J.; Zezin, A. B.; Müller, A. H. E.; Kabanov, V. A. *Polymer* **2004**, *45*, 367−378.
(8) Schuch, H.; Klingler, J.; Rossmanith, P.; Frechen, T.; Gerst, M.; Feldthusen, J.; Müller, A. H. E. *Macromolecules* **2000**, *33*, 1734−1740.
(9) Burguière, C.; Chassenieux, C.; Charleux, B. *Polymer* **2003**, *44*, 509−518.

(10) Astafieva, I.; Khougaz, K.; Eisenberg, A. *Macromolecules* **1995**, *28*, 7127−7134.
(11) Lindner, H.; Glatter, O. *Part. Part. Syst. Charact.* **2000**, *17*, 89−95.
(12) Schulz, G. V. *Z. Phys. Chem. B* **1939**, *43*, 25.
(13) Burchard, W. *Adv. Polym. Sci.* **1999**, *143*, 113−194.
(14) Förster, S.; Zisenis, M.; Wenz, E.; Antonietti, M. *J. Chem. Phys.* **1996**, *104*, 9956−9970.
(15) van der Maarel, J. R. C.; Groenewegen, W.; Egelhaaf, S. U.; Lapp, A. *Langmuir* **2000**, *16*, 7510−7519.
(16) Stepanek, M.; Krijtova, K.; Limpouchova, Z.; Prochazka, K.; Teng, Y.; Munk, P.; Webber, S. E. *Acta Polym.* **1998**, *49*, 103.
(17) Stepanek, M.; Podhajecka, K.; Prochazka, K.; Teng, Y.; Webber, S. E. *Langmuir* **1999**, *15*, 4185−4193.
(18) Stepanek, M.; Prochazka, K.; Brown, W. *Langmuir* **2000**, *16*, 2502.
(19) Teng, Y.; Morrison, M. E.; Munk, P.; Webber, S. E.; Prochazka, K. *Macromolecules* **1998**, *31*, 3578−3587.
(20) Uhlik, F.; Limpouchova, Z.; Jelinek, K.; Prochazka, K. *J. Chem. Phys.* **2004**, *121*, 2367.
(21) Matejicek, P.; Uhlik, F.; Limpouchova, Z.; Prochazka, K.; Tuzar, Z. *Macromolecules* **2002**, *35*, 9487.
(22) Besseling, N. A. M.; Cohen Stuart, M. A. *J. Chem. Phys.* **1999**, *110*, 5432−5436.
(23) Talanquer, V.; Oxtoby, D. W. *J. Chem. Phys.* **2000**, *113*, 7013−7021.
(24) Nyrkova, I. A.; Semenov, A. N. *Faraday Discuss.* **2005**, *128*, 113−127.
(25) Nyrkova, I. A.; Semenov, A. N. *Macromol. Theory Simul.* **2005**, *14*, 569−585.
(26) Garnier, S.; Laschewsky, A. *Macromolecules* **2005**, *38*, 7580−7592.
(27) Martin, T. J.; Prochazka, K.; Munk, P.; Webber, S. E. *Macromolecules* **1996**, *29*, 6071−6073.

MA0609580